# Optical studies of the $a$-, $b$-, and $c$-axis charge dynamics in $YBa_2Cu_3O_{6+x}$

S. L. Cooper, D. Reznik, A. Kotz, M. A. Karlow, R. Liu, M. V. Klein,
W. C. Lee, J. Giapintzakis, and D. M. Ginsberg
*Department of Physics and Materials Research Laboratory, University of Illinois at Urbana-Champaign, 1110 West Green Street, Urbana, Illinois 61801*

B. W. Veal and A. P. Paulikas
*Materials Science Division, Argonne National Laboratory, Argonne, Illinois 60439*
(Received 3 September 1992; revised manuscript received 13 November 1992)

Optical and Raman-scattering studies of $a$-, $b$-, and $c$-axis $YBa_2Cu_3O_{6+x}$ between 0.025 and 5.5 eV are presented as a function of doping, and compared to the results of $Bi_2Sr_2CaCu_2O_8$ and $La_{2-x}Sr_xCuO_4$. Our doping-dependence studies show that the redistribution of spectral weight in the $CuO_2$ planes of $YBa_2Cu_3O_{6+x}$ differs significantly from that seen in $La_{2-x}Sr_xCuO_4$. We also find that the redistribution of spectral weight in the cuprates is primarily responsible for the loss of two-magnon Raman-scattering intensity with doping. Finally, we show that bound-carrier contributions comprise a significantly larger fraction of the spectral weight below 1 eV in lower-$T_c$ cuprates such as the 2:1:4 compounds than in higher-$T_c$ cuprates such as $YBa_2Cu_3O_{6+x}$ and $Bi_2Sr_2CaCu_2O_8$. We suggest that the low-frequency conductivity ( $<1$ eV) in the 2:1:4 compounds is most appropriately described by a two-component picture, while that in $YBa_2Cu_3O_{6+x}$ and $Bi_2Sr_2CaCu_2O_8$ is adequately described as a single component of strongly interacting carriers. In the metallic phase we find several interesting consequences of a single-component interpretation of the optical data in $YBa_2Cu_3O_{6+x}$, such as a linear-in-$\omega$ frequency-dependent scattering rate and an increase in the interaction strength with decreased carrier density. Finally, we show that the $c$-axis optical response in $YBa_2Cu_3O_7$ ($T_c \sim 90$ K) is characterized by a $c$-axis polarized Raman continuum and a Drude conductivity arising from interbilayer charge transport along the $c$ direction. With decreased doping, the $c$-axis Drude response decreases dramatically, indicating a decoupling of the $CuO_2$ plane bilayers in $YBa_2Cu_3O_{6+x}$. By comparison, the $ab$-plane optical response is not strongly influenced by interbilayer decoupling, suggesting that the unusual $ab$-plane charge dynamics in $YBa_2Cu_3O_{6+x}$ persist in nearly isolated $CuO_2$ plane bilayers.

## I. INTRODUCTION

In spite of much study, a number of uncertainties regarding the nature of the normal-state charge dynamics in the high-$T_c$ cuprates remain. For example, the evolution of the optical response in the $CuO_2$ planes with doping is still not well understood. Optical studies of 2:1:4 compounds such as $La_{2-x}Sr_xCuO_4$ (Ref. 1) and $Pr_{2-x}Ce_xCuO_4$ (Ref. 2) show that both Drude-like and mid-infrared absorption bands develop with doping at the expense of oscillator strength above the charge-transfer gap. However, determining whether this behavior characterizes the intrinsic $CuO_2$ plane optical response in the high-$T_c$ cuprates in general has been difficult in twinned $YBa_2Cu_3O_{6+x}$, due to the presence of CuO chain contributions to the optical response. Secondly, an appropriate description for the unusual charge dynamics in the metallic phase, characterized by a non-Drude optical conductivity below 1 eV (Ref. 3), and a broad inelastic Raman-scattering continuum,[4–6] has not yet been established. The low-frequency optical response in the cuprates has been described both by single-component models, in which non-Drude behavior is attributed to quasiparticle damping effects, and by two-component models, in which the unusual optical response is ascribed to the presence of secondary absorption processes unrelated to the free carriers. Again, this issue has been difficult to clarify in studies of twinned $YBa_2Cu_3O_{6+x}$ due to the presence of the CuO chains. Finally, it has not yet been determined if $c$-axis transport in the cuprates is coherent. This issue is particularly significant, as it confronts the basic assumptions made by both normal and superconducting state models of the cuprates.

In this paper, we report optical reflectivity, ellipsometry, and Raman-scattering measurements of $Bi_2Sr_2CaCu_2O_8$ and twinned and single-domain $YBa_2Cu_3O_{6+x}$. The motivation behind this study is twofold. First, by examining the relationship between the Raman scattering and optical responses in $a$-, $b$-, and $c$-axis $YBa_2Cu_3O_{6+x}$, we hope to gain more insight into the nature of the charge and spin dynamics in this material. Secondly, by isolating the intrinsic $CuO_2$ plane response in single-domain $YBa_2Cu_3O_{6+x}$, we can make meaningful comparisons of the charge dynamics in the $CuO_2$ planes of different cuprates. In particular, we can examine the extent to which the $CuO_2$ plane charge dynamics of the high-$T_c$ cuprates exhibit universal characteristics.

Section II describes details of the sample preparation, the various experimental techniques used, and the procedure used to combine optical reflectivity and ellipsometric data to obtain accurate optical functions between 0.02 and 5.5 eV.

 

Section III presents our reflectivity and Raman-scattering results for *ab*-plane $YBa_2Cu_3O_{6+x}$ and $Bi_2Sr_2CaCu_2O_8$, and examines a variety of spectral functions obtained from a Kramers-Kronig analysis of the reflectivity data. Results on twinned $YBa_2Cu_3O_{6+x}$ samples at a variety of concentrations are juxtaposed with single-domain $YBa_2Cu_3O_{6+x}$ results at several concentrations in order to isolate $CuO_2$ plane contributions to the optical response.

Section IV A discusses the doping dependence of the *ab*-plane optical response of various cuprates, focusing in particular on $CuO_2$ plane contributions in $YBa_2Cu_3O_{6+x}$. Among our chief observations, we find that spectral weight in the charge-transfer absorption band decreases dramatically with doping, in agreement with Hubbard model predictions. Additionally, we show that the composition of the low-frequency spectral weight in different cuprates varies significantly, with bound-carrier contributions comprising a substantially larger fraction of spectral weight below 1 eV in the 2:1:4 cuprates than in $YBa_2Cu_3O_{6+x}$ and $Bi_2Sr_2CaCu_2O_8$. This leads us to suggest that the 2:1:4 compounds must be described by a two-component picture involving both bound and mobile charges, while the low-frequency conductivity in $YBa_2Cu_3O_{6+x}$ and $Bi_2Sr_2CaCu_2O_8$ is adequately described as a single component of mobile carriers.

Section IV B presents the results of a single-component analysis of the optical data in $YBa_2Cu_3O_{6+x}$ and $Bi_2Sr_2CaCu_2O_8$, and examines the physical consequences of these results. We find that within a single-component model, the doping dependence of the optical conductivity is consistent with an increase in the quasiparticle interaction strength with decreasing carrier concentration. Furthermore, the dependence of the Raman-scattering spectra on doping places strong constraints on the possible relationship between the optical response and the unusual Raman-scattering continuum.

Section V presents and discusses our *c*-axis optical results as a function of doping. We find that the *c*-axis optical response of $YBa_2Cu_3O_7$ ($T_c \sim 90$ K) is characterized by both a small Drude term arising from interbilayer charge transport, and a *c*-axis polarized Raman continuum. With decreased doping, we find that the disruption of the CuO chains by removing oxygen from the chain sites causes a rapid decoupling of adjacent $CuO_2$ plane bilayers. Notably, the *ab*-plane optical response appears to be relatively unaffected by interbilayer decoupling, providing strong evidence that the unusual normal-state charge dynamics of *ab*-plane $YBa_2Cu_3O_{6+x}$ persists in decoupled $CuO_2$ bilayers.

## II. EXPERIMENTAL

### A. Sample preparation

$Bi_2Sr_2CaCu_2O_8$, single-domain $YBa_2Cu_3O_{6+x}$, and twinned $YBa_2Cu_3O_{6+x}$ crystals were used in this study. The $T_c = 90$ K ($x \sim 1$) single-domain $YBa_2Cu_3O_{6+x}$ samples are grown using a method described elsewhere.[7] Single domain $YBa_2Cu_3O_{6+x}$ crystals with $T_c = 66$ K ($x \sim 0.6$) are grown by annealing as-grown tetragonal single crystals in flowing oxygen at 650 °C for ten days, then rapidly quenching the samples down to liquid-nitrogen temperatures within a few seconds.[8] Insulating $YBa_2Cu_3O_{6.1}$ crystals are prepared by annealing the as-grown crystals in flowing nitrogen gas at 650 °C for two days, then rapidly quenching the samples down to liquid-nitrogen temperatures. The magnetization measurements for the 66 and 90 K crystals used in this study are shown in Fig. 1(a), illustrating superconducting transition widths (defined as the temperature difference between 10 and 90% maximum Meissner effect value) of 2 and 5 K for the 90 and 66 K single-domain crystals, respectively.

Twinned *ab*-plane $YBa_2Cu_3O_{6+x}$ samples with $x \sim 0.9$ ($T_c = 91$ K), 0.8 ($T_c = 85$ K), 0.5 ($T_c = 54$ K), 0.4 ($T_c = 38$ K), and 0.3 ($T_c = 0$ K), and thick *c*-axis samples with $x \sim 1$ ($T_c = 91$ K), 0.8 ($T_c = 81$ K), and 0.7 ($T_c = 70$ K) were grown in gold crucibles using a method described elsewhere.[9] The magnetization measurements for the twinned crystals are shown in Fig. 1(b), illustrating the sharp transition widths exhibited by all of the superconducting samples measured.

### B. Reflectivity and ellipsometry measurements

Optical reflectivity measurements between 0.02 and 5.5 eV were obtained in a near-normal incidence config-

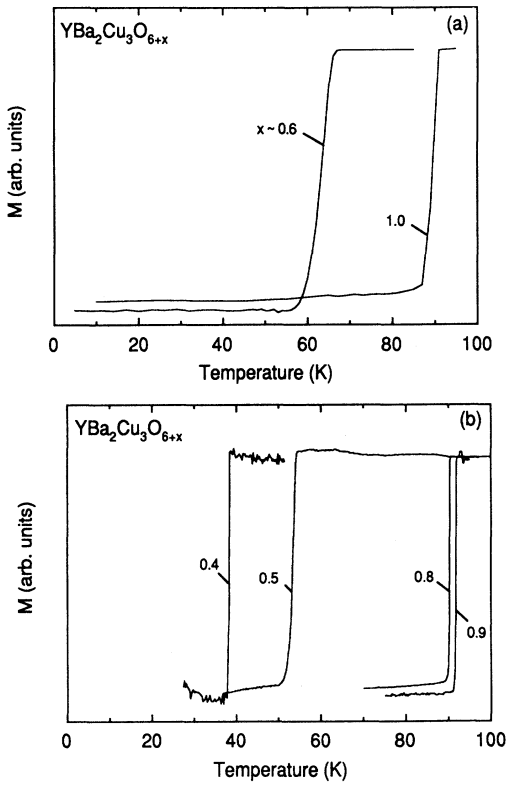


FIG. 1. Bulk magnetization vs temperature in (a) single domain and (b) twinned samples of $YBa_2Cu_3O_{6+x}$. The vertical scale is plotted in arbitrary units. The curves in (b) have been scaled by factors of 8.6 ($x \sim 0.4$), 2.4 ($x \sim 0.5$), 1 ($x \sim 0.8$), and 38 ($x \sim 0.9$).

uration with a rapid scanning interferometer. The modulated light beam from the interferometer was refocused onto either the sample or an Au (for $0<\omega<2$ eV) or Al (for $1.5<\omega<5.5$ eV) reference mirror, and the reflected beam was refocused onto a detector appropriate for the frequency range studied. The different sources, polarizers, and detectors used in these studies provided substantial spectral overlap, and the reflectivity mismatch between adjacent spectral ranges was less than 1%.

Ellipsometry measurements were also made between 1.5 and 6 eV using a rotating analyzer ellipsometer. A 75 W xenon arc lamp was used as the broad band source for the ellipsometer, and wavelength selection was made with a Cary monochromator. The incident polarization state was selected by a Rochon prism acting as a polarizer. After reflection from the sample at a known angle, the polarization state of the light was sampled by a rotating Rochon prism acting as an analyzer, and the light intensity was detected with a current mode photomultiplier tube.

### C. Phase correction procedure

One of the most common methods for obtaining the frequency-dependent dielectric response is to use the measured reflectivity $R(\omega)$, and the phase $\Theta(\omega)$ estimated from a Kramers-Kronig transformation of $R(\omega)$,

$$\Theta(\omega)=\frac{\omega}{\pi}\int_0^\infty \frac{\ln R(\omega')-\ln R(\omega)}{\omega^2-\omega'^2}d\omega' , \quad (1)$$

to calculate other fundamental optical constants.[10] Unfortunately, the Kramers-Kronig integral requires knowledge of the reflectivity at all frequencies, and therefore $R$ must be extrapolated beyond the measured frequency range. The uncertainties in these extrapolations can result in large errors in $\Theta$ which are subsequently propagated in the calculation of the dielectric response.

Recently, Bozovic[11] introduced a procedure in which errors in $\Theta$ resulting from a Kramers-Kronig transformation of limited reflectivity data are corrected using the exact $\Theta$ determined from ellipsometric techniques. Below, we describe a modified version of this procedure which has been employed in the present study to obtain accurate values of the optical constants in $Bi_2Sr_2CaCu_2O_8$ and $YBa_2Cu_3O_{6+x}$ between 0.025 and 5.5 eV.

In Fig. 2 we illustrate our correction procedure for a twinned $YBa_2Cu_3O_{6.9}$ sample ($T_c=90$ K). Figure 2(a) exhibits the reflectivity spectra obtained both from direct reflectivity measurements (solid line) and from ellipsometry measurements (open circles). The agreement between the reflectivity and ellipsometry results is better than 2%. To obtain the optical constants in these materials, we first calculate the phase $\Theta$ of the complex reflectance from our reflectivity data using the Kramers-Kronig relation in Eq. (1). The reflectivity data are extrapolated above 5.5 eV using the form

$$R_{\text{extrap}}=R_\infty+(R_u-R_\infty)\left[\frac{\omega_u}{\omega}\right]^\alpha , \quad (2)$$

where $R_u$ and $\omega_u$ are the reflectivity and frequency at the upper limit of the measured data, and $R_\infty$ and $\alpha$ ($0<\alpha<4$) are the high-frequency reflectivity and power of the frequency dependence. $R_\infty$ and $\alpha$ are treated as adjustable parameters in order that the phase calculated from the Kramers-Kronig analysis, $\Theta_{KK}$, gives the best possible match to the low-frequency part of the exact phase determined from ellipsometry measurements, $\Theta_{\text{ellip}}$. As an example, Fig. 2(b) compares the phase obtained from this Kramers-Kronig transformation of the reflectivity in Fig. 2(a) (dashed line) with the ellipsometrically derived result (open circles). Above roughly 4 eV, the Kramers-Kronig derived phase $\Theta_{KK}$ is forced to match the ellipsometric phase, giving the total corrected phase, $\Theta_{\text{corr}}$ (solid line). Notably, the corrected phase can differ substantially from phase angles obtained using arbi-

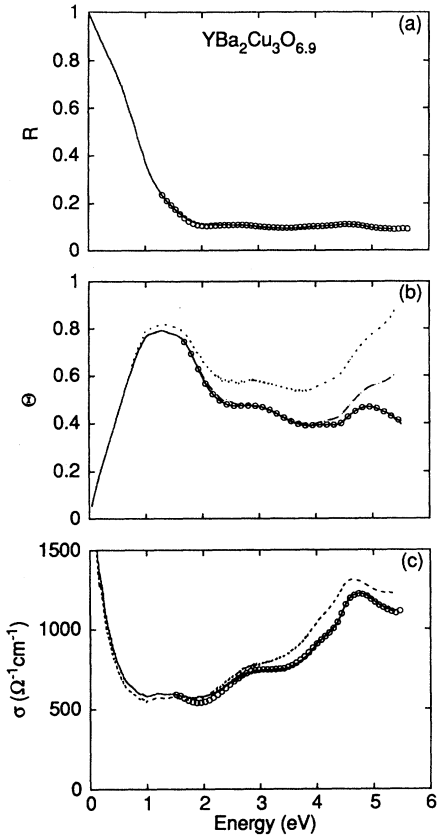


FIG. 2. (a) The solid line shows the room-temperature reflectivity $R$ of twinned $YBa_2Cu_3O_{6.9}$. The open circles compare the reflectivity obtained from ellipsometric results. (b) The dash-dotted line illustrates the phase angle $\Theta(\omega)$ obtained from a Kramers-Kronig transformation of the reflectivity in (a). The solid line illustrates $\Theta(\omega)$ obtained via the correction procedure described in the text. The exact ellipsometric result is illustrated by the open circles. The dotted line compares the $\Theta(\omega)$ obtained from a Kramers-Kronig analysis of the reflectivity in (a), using a $\omega^{-4}$ extrapolation. (c) The solid line shows the real part of the optical conductivity $\sigma(\omega)$ obtained from the phase correction procedure described in the text. The exact ellipsometric result is illustrated by the open circles. The dashed line compares the $\sigma(\omega)$ obtained from the reflectance in (a) and the arbitrary phase angle shown in (b) (dotted line).

trary extrapolations, as illustrated by the phase obtained with a $\omega^{-4}$ extrapolation in Fig. 2(b) (dotted line).

In the final step of our correction procedure, various optical functions are determined between 0.02 and 5.5 eV using the measured $R$, the corrected phase angle $\Theta_{corr}$, and standard constitutive relations.[10] As demonstrated by the calculated conductivity (solid line) in Fig. 2(c), the results of this procedure are optical functions between 0.02 and 5.5 eV that match with the exact ellipsometric results above 1.5 eV (open circles). By contrast, the conductivity obtained from arbitrary extrapolations (dashed line) can differ substantially from the ellipsometric result.

### D. Raman-scattering measurements

Raman-scattering measurements on both twinned and single-domain samples of $YBa_2Cu_3O_{6+x}$ were also made at 300 K using a Spex Triplemate Raman Spectrometer equipped with a nitrogen-cooled CCD array detector. All spectra were corrected for the frequency response of the spectrometer and the detector. Because of the wide frequency range of our scans, artificial intensity loss in the spectra can result from a gradual defocusing of the image at the entrance slit due to chromatic aberration. To avoid this, the entrance slit was underfilled with the laser spot image. It is also essential to obtain the absolute Raman-scattering cross section when comparing the Raman spectra at different doping levels. Therefore, the Raman spectra were corrected for the optical absorption of the samples and the refraction at the sample-air interface using a procedure described elsewhere.[12]

## III. *ab*-PLANE OPTICAL RESPONSE: RESULTS

### A. Insulating phase

Many of the chief properties of the insulating cuprates, such as the presence of antiferromagnetism and an energy gap, are thought to be well described by the three-band Hubbard model. This model distills the complicated band structure of the cuprates into three essential orbital contributions, the Cu(2) $d_{x^2-y^2}$ band, which is split into upper and lower Hubbard bands by a large on-site Coulomb repulsion $U \sim 8-10$ eV, and the O(2,3) $p_{x,y}$ bands, which lie a "charge-transfer" energy, $\Delta = (\varepsilon_p - \varepsilon_d)$, below the upper Hubbard band. Because the fundamental absorption gap in the cuprates occurs between the filled O(2,3) $p_{x,y}$ charge-transfer band and the empty upper Hubbard band, i.e., $E_g \sim \Delta$, the cuprates are classified as charge-transfer insulators ($U \gg \Delta$).[13] In the opposite, Mott-Hubbard limit, the charge-transfer energy exceeds the on-site Coulomb repulsion ($U \ll \Delta$), and the fundamental absorption gap occurs between the upper and lower Hubbard bands. High-energy spectroscopic studies of the cuprates appear to support the main features of the charge-transfer model, demonstrating for example that the lowest unoccupied band is chiefly comprised of Cu(2) $d_{x^2-y^2}$ states while the highest occupied band consists primarily of O(2,3) $p_{x,y}$ states.[14]

The detailed low-frequency structure of the fundamental absorption gap in insulating $YBa_2Cu_3O_{6.1}$ is illustrated by the optical reflectivity and conductivity in Figs. 3(a) and 3(b), respectively (solid lines). For comparison, we also show the reflectivity and conductivity of a more structurally simple cuprate,[15] $T'$-phase $Gd_2CuO_4$ in Fig. 3 (dashed lines), in order to identify characteristic $CuO_2$ plane contributions to the optical response. The conductivities of both $YBa_2Cu_3O_{6.1}$ and $Gd_2CuO_4$ exhibit a fundamental absorption edge near $\Delta = 1.75$ eV, which has been generally attributed to the charge-transfer energy required to transfer a hole between the Cu(2) $d_{x^2-y^2}$ and O(2,3) $p_{x,y}$ sites on the $CuO_2$ planes.[16–20] $YBa_2Cu_3O_{6.1}$ also exhibits a strong transition at 4.1 eV which is not believed to be a $CuO_2$ plane transition, due in part to its absence in $T'$-phase materials such as $Gd_2CuO_4$. The 4.1 eV feature has been attributed to several out-of-plane transitions, including $3d_{3z2-1}$ to $4p_{x,y}$ transitions on the Cu(1) site,[21] Cu(1)-O(4) transitions,[22] and excitations in the Ba-O(4) plane.[23] $Gd_2CuO_4$ also shows a higher energy transition near 5 eV, which has been attributed to charge-transfer transitions involving Cu(4*d*)-O(3*s*) states.[24]

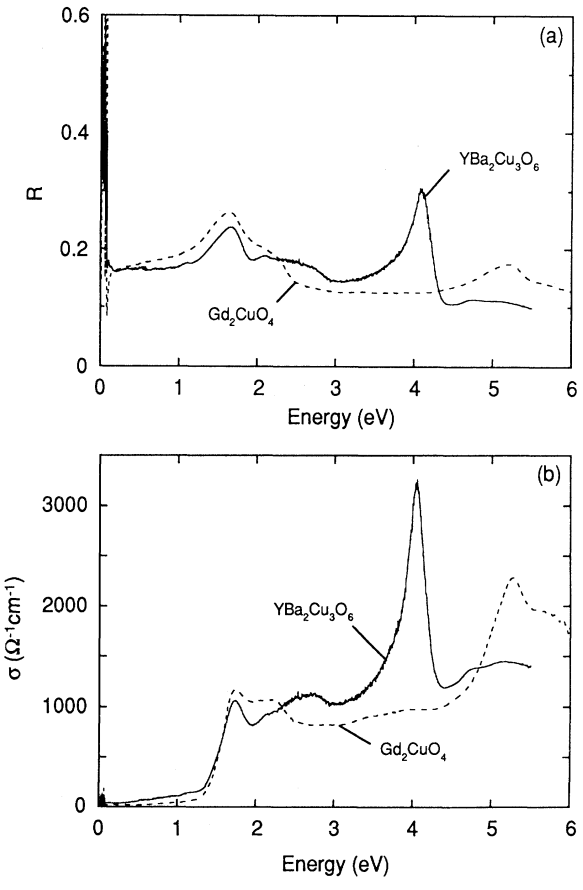


FIG. 3. (a) Room-temperature reflectance data of insulating compounds $YBa_2Cu_3O_{6.1}$ (solid line) and $T'$-phase $Gd_2CuO_4$ (dashed line). (b) Real part of the optical conductivity for $YBa_2Cu_3O_{6.1}$ (solid line) and $Gd_2CuO_4$ (dashed line).

### B. Doping dependence in the *ab* plane

#### *1. Reflectivity*

The development of the room-temperature optical reflectivity $R$ in twinned $YBa_2Cu_3O_{6+x}$ with doping is illustrated in Fig. 4(a). Among the trends observed in $R$ with increased doping are a loss of spectral weight above the charge-transfer gap, and the development of a plasma edge that moves to higher energies with increasing $x$. Figure 4(a) also shows that there is a systematic loss of reflected intensity between 1.5 and 5 eV with increased doping.

In order to isolate $a$-axis and $b$-axis contributions in $YBa_2Cu_3O_{6+x}$, reflectivity measurements on single-domain samples are shown in Fig. 4(b) for the electric field polarized parallel to the $a$ axis (solid lines, $\mathbf{E}\perp$CuO chains) and the $b$ axis (dashed lines, $\mathbf{E}\|$CuO chains). In addition to the trends observed in twinned $YBa_2Cu_3O_{6+x}$ [Fig. 4(a)], a large optical anisotropy is observed between the $a$- and $b$-axis reflectivity, indicating a substantial contribution of the CuO chains to the optical response. Similar results have been described previously in optical measurements of single-domain $YBa_2Cu_3O_7$ [25–29] and $YBa_2Cu_3O_{6.6}$.[28,29]

Notably, the intrinsic $CuO_2$ plane optical reflectivities in the metallic phase of both $a$-axis $YBa_2Cu_3O_{6+x}$ and $Bi_2Sr_2CaCu_2O_8$ [dashed-dotted line in Fig. 4(b)] are characterized by a quasilinear dependence on frequency. By contrast, the $b$-axis reflectivities of $YBa_2Cu_3O_{6+x}$ (dashed lines) are nonlinear and have substantially higher plasma edges, presumably reflecting the large contribution of CuO chain states.

#### *2. Optical conductivity*

The frequency-dependent conductivities $\sigma$ of $YBa_2Cu_3O_{6+x}$, derived from the reflectivity spectra in Fig. 4, are shown in Fig. 5 for (a) twinned and (b) single-domain samples. As suggested by the reflectivity data in Fig. 4, spectral weight throughout the 1.5 to 5 eV region systematically decreases with doping up to $x\sim0.5$, while conductivity below 1.5 eV grows significantly throughout the doping range. Significantly, the low-frequency spectral weight grows somewhat faster than the dopant concentration, $x$ (see discussion, Sec. IV A 1), suggesting that weight lost above the charge-transfer absorption band is transferred to low energies with doping.[28] Similar results have also been reported in several 2:1:4 compounds.[1,2]

The conductivity below 1.5 eV in *twinned*

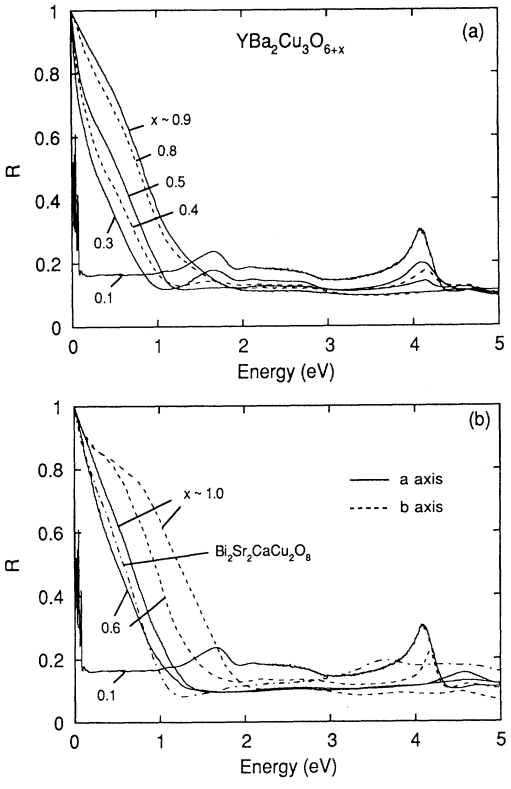


FIG. 4. (a) Room-temperature reflectivity data of twinned $YBa_2Cu_3O_{6+x}$ for various $x$. (b) Room-temperature reflectivity data of single-domain $YBa_2Cu_3O_{6+x}$ at various $x$ for $\mathbf{E}\|a$ axis (solid lines) and $\mathbf{E}\|b$ axis (dashed lines). The dashed-dotted line compares the reflectivity of $Bi_2Sr_2CaCu_2O_8$.

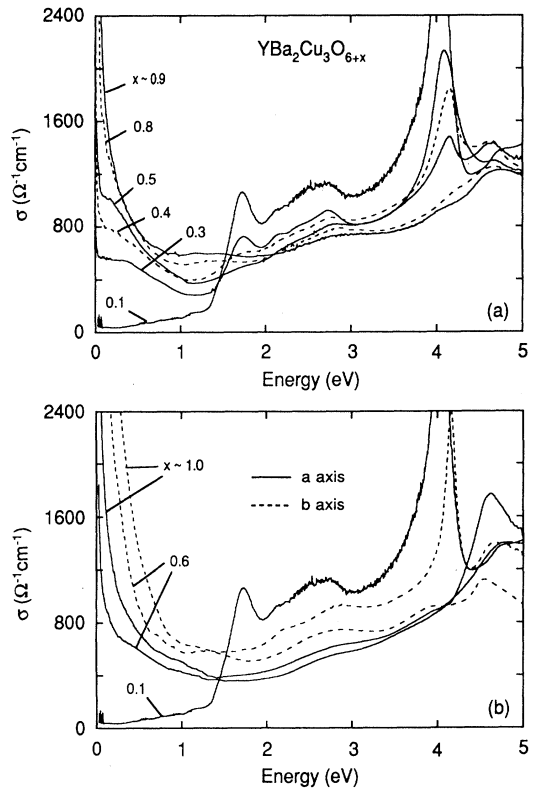


FIG. 5. (a) Real part of the optical conductivity $\sigma(\omega)$ of twinned $YBa_2Cu_3O_{6+x}$ for various $x$. (b) $\sigma(\omega)$ of single-domain $YBa_2Cu_3O_{6+x}$ at various $x$ for $\mathbf{E}\|a$ axis (solid lines) and $\mathbf{E}\|b$ axis (dashed lines).

$YBa_2Cu_3O_{6+x}$ crystals evolves into two distinct components,[30] including a Drude-like contribution centered at $\omega=0$, and a mid-infrared absorption band near 0.5 eV that systematically shifts to lower frequencies with increased doping. In order to identify $CuO_2$ plane and CuO chain contributions to the two-component low-frequency conductivity in twinned $YBa_2Cu_3O_{6+x}$, we show the *a*-axis (solid lines) and *b*-axis (dashed lines) conductivities of single-domain $YBa_2Cu_3O_{6+x}$ as a function of doping in Fig. 5(b). At low frequencies, the *a*-axis optical conductivity in metallic $YBa_2Cu_3O_{6+x}$ should represent the conductivity associated with the $CuO_2$ planes alone. This conclusion is indeed supported by the strong similarity between the conductivities of *a*-axis $YBa_2Cu_3O_7$ and chainless $Bi_2Sr_2CaCu_2O_8$ below 1 eV in Fig. 6. Consequently, in the following we associate the *a*-axis optical response below 1 eV in $YBa_2Cu_3O_{6+x}$ with the $CuO_2$ plane contribution, and the *b*-axis response with a combination of $CuO_2$ plane and CuO chain contributions.

The development of $\sigma$ with doping in *a*-axis $YBa_2Cu_3O_{6+x}$ (solid lines) exhibits the same loss of spectral weight above 1.5 eV observed in the twinned data. However, the *a*-axis conductivity (solid lines) *does not* exhibit a resolvable mid-infrared absorption band, in contrast to the results of twinned $YBa_2Cu_3O_{6+x}$ measurements. This result supports the conclusion that the mid-infrared absorption band in twinned $YBa_2Cu_3O_{6+x}$ principally arises from CuO chain contributions.[27] Indeed, Fig. 6 compares the $CuO_2$ plane (i.e., *a* axis) conductivity below 1 eV (solid lines) to a rough estimate of the CuO chain contribution to the conductivity $\sigma_b$-$\sigma_a$ (dashed lines), demonstrating that much of the prominent mid-infrared peak observed in the metallic phase of twinning samples arises from CuO chain contributions. Further, the conductivity of $Bi_2Sr_2CaCu_2O_8$ in Fig. 6 (dashed-dotted line) shows no evidence for a mid-infrared absorption band, providing additional evidence that the distinct mid-infrared absorption band in twinned $YBa_2Cu_3O_{6+x}$ is not an intrinsic feature of the $CuO_2$ planes.

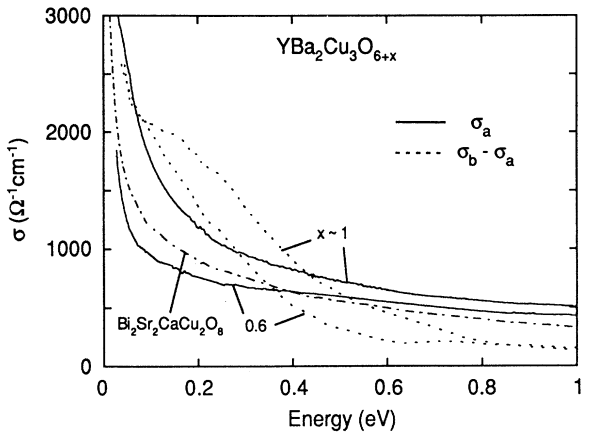


FIG. 6. Real part of the optical conductivity $\sigma$ below 1 eV in the $CuO_2$ planes [$=a$ axis] of single-domain $YBa_2Cu_3O_{6+x}$ (solid lines), compared with an estimate of the conductivity associated with the CuO chains [$=\sigma_b-\sigma_a$] (dotted lines). The dashed-dotted line compares the conductivity of $Bi_2Sr_2CaCu_2O_8$.

Significantly, the low-frequency $CuO_2$ plane conductivities of metallic $YBa_2Cu_3O_{6+x}$ and $Bi_2Sr_2CaCu_2O_8$ fall off more slowly with frequency ($\sigma\sim\omega^{-1}$) than a simple Drude response ($\sigma\sim\omega^{-2}$) (see Fig. 6).[28,29] As discussed in Sec. IV B 1, this non-Drude behavior suggests the presence of either frequency-dependent carrier scattering[3] or a mid-infrared absorption band that cannot be resolved from the Drude response.

### 3. *Effective electron number*

A more quantitative analysis of the distribution of spectral weight between the CuO planes and chains of $YBa_2Cu_3O_{6+x}$ is afforded by examining the spectral function

$$N_{\rm eff}(\omega)=\frac{2mV_{\rm cell}}{\pi e^2}\int_0^{\omega}\sigma(\omega')d\omega' , \tag{3}$$

where $(m/m^*)N_{\rm eff}(\omega)$ is the effective number of electrons per unit cell contributing to the conductivity below $\omega$, $m$ and $e$ are the bare electron mass and charge, respectively, $m^*$ is the renormalized electron mass, and $V_{\rm cell}$ is the unit cell volume. $N_{\rm eff}(\omega_0)$ provides a measure of the integrated spectral weight in the conductivity up to an arbitrary frequency $\omega_0$, and is related to an equivalent plasma frequency in $YBa_2Cu_3O_{6+x}$ by the relationship

$$\omega_p^2(eV^2)=\frac{4\pi e^2}{m^*}\frac{N_{\rm eff}(\omega_0)}{V_{\rm cell}}\sim 8N_{\rm eff}(\omega_0) . \tag{4}$$

The resulting $N_{\rm eff}$ functions for twinned $YBa_2Cu_3O_{6+x}$ samples are illustrated in Fig. 7(a). In the insulating phase, $N_{\rm eff}$ remains near zero throughout the conductivity gap, but increases rapidly above the fundamental absorption edge near 1.5 eV. In the metallic phase, $N_{\rm eff}$ exhibits a rapid rise at low frequencies due to the appearance of a Drude-like band centered at $\omega=0$.

In order to distinguish chain and plane contributions to $N_{\rm eff}$, we plot $N_{\rm eff}$ from the *a*-axis [$=CuO_2$ panel] (solid lines) and *b*-axis [$=CuO_2$ plane + CuO chain] (dashed lines) conductivities in Fig. 7(b). Notably, the integrated spectral weight associated with the $CuO_2$ planes of metallic $YBa_2Cu_2O_{6.6}$ in Fig. 7(b) intersects that of insulating $YBa_2Cu_3O_{6.1}$ near 3 eV. This implies that while the *total* spectral weight below 3 eV is not affected by doping, there is a transfer of spectral weight from the charge-transfer band region (1.5–3 eV) to low frequencies ($<1.5$ eV) with increased doping. Similar results have been reported in several 2:1:4 compounds.[1,2] Additionally, a comparison of *a*-axis [$CuO_2$ planes] and *b*-axis [CuO planes + chains] contributions to $N_{\rm eff}$ illustrates that the $CuO_2$ planes (solid lines) contain half of the total (i.e., CuO plane + chain) spectral weight, with the balance residing on the CuO chains.

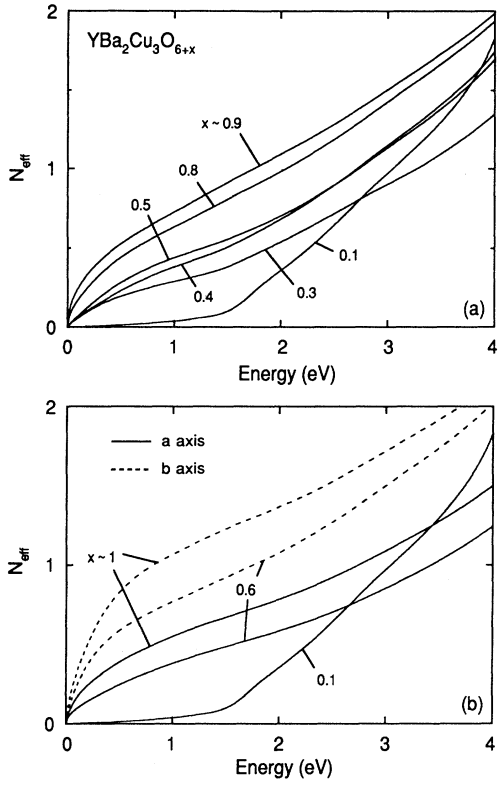


FIG. 7. (a) Number of effective carriers $N_{\text{eff}}$ in twinned $YBa_2Cu_3O_{6+x}$ for various $x$, obtained from an integration of the conductivity using Eq. (3). (b) $N_{\text{eff}}$ in single-domain $YBa_2Cu_3O_{6+x}$ at various $x$ for $\mathbf{E}\|a$ axis (solid lines) and $\mathbf{E}\|b$ axis (dashed lines).

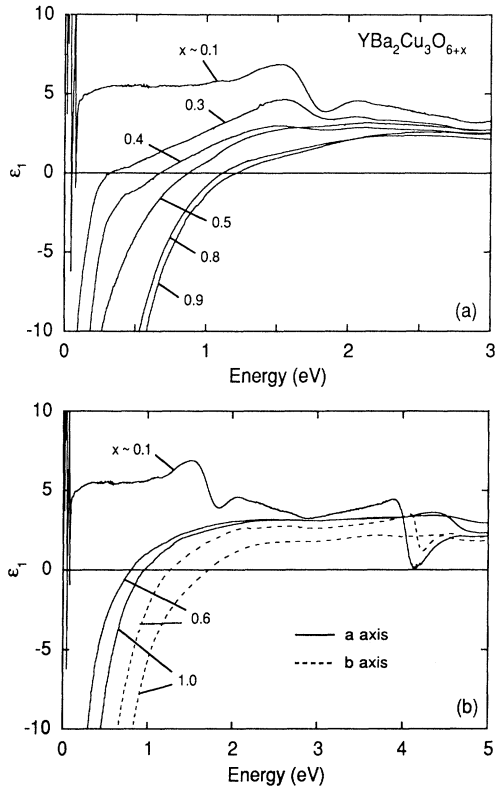


FIG. 8. (a) Real part of the dielectric response $\epsilon_1$ in twinned $YBa_2Cu_3O_{6+x}$ for various $x$. (b) $\epsilon_1$ in single-domain $YBa_2Cu_3O_{6+x}$ for various $x$ with $\mathbf{E}\|a$ axis (solid lines) and $\mathbf{E}\|b$ axis (dashed lines).

#### 4. *Dielectric function*

In Fig. 8(a), the real part of the dielectric function $\varepsilon_1$ is illustrated as a function of doping for twinned $YBa_2Cu_3O_{6+x}$, exhibiting a systematic increase in the zero crossing with increased doping. In a simple Drude model, the frequency $\omega_0$ at which the real part of the dielectric function crosses zero $\varepsilon_1(\omega_0)$ is related to the free-carrier plasma frequency by $\omega_0^2=\omega_p^2+1/\tau^2$, where $\tau$ is the relaxation rate of the carriers. Consequently, an increase of $\varepsilon_1(\omega_0)$ with doping in a Drude system reflects increases in $\omega_p^2$ and the carrier density. As discussed below (Sec. IV A 2), the presence of bound carriers in the cuprates complicates this simple picture, by contributing a positive dielectric response that dielectrically screens the free-carrier response and lowers $\varepsilon_1(\omega_0)$.

Figure 8(b) displays the *a*-axis (solid lines) and *b*-axis (dashed lines) contributions to $\varepsilon_1$ as a function of doping. These spectra illustrate that the effective plasma frequency in the *b* direction is larger than that along the *a* direction due to the presence of CuO chain contributions. Both *a*- and *b*-axis contributions exhibit a systematic shift of $\varepsilon_1(\omega_0)$ with doping, consistent with the results of twinned $YBa_2Cu_3O_{6+x}$ measurements. Moreover, the larger shift in $\varepsilon_{1b}(\omega_0)$ between $x=0.6$ and $x=1$ indicates that spectral weight in the CuO chains increases with doping as much as that on the $CuO_2$ planes.

#### 5. *Raman scattering*

The Raman-scattering spectra of single-domain $YBa_2Cu_3O_{6+x}$ are illustrated for several oxygen concentrations in Fig. 9(a), exhibiting two-magnon scattering in the insulating phase,[31] and broad continuum scattering in the metallic phase.[4–6] The doping dependence in Fig. 9(a) illustrates several interesting features. First, the Raman continuum is clearly larger along the *b* axis (yy), possibly due to the presence of interband CuO chain contributions to the Raman-scattering response.

Secondly, the Cu-O plane polarized Raman-scattering continuum appears to be *insensitive* to doping. This doping independence is in sharp contrast to the substantial growth in the low-frequency optical conductivity with increased doping (see Fig. 6). As we discuss in Sec. IV B 2, this discrepancy places important conditions on the possible relationship between the Raman-scattering continuum and the low-frequency optical conductivity.

Finally, the two-magnon spectrum decreases dramatically with doping, and is not observed in the metallic phase in agreement with earlier results on twinned crystals.[32] Figure 9(b) illustrates in greater detail the decrease of two-magnon scattering with doping in $YBa_2Cu_3O_{6+x}$. There are several indications that the strong doping dependence of the two-magnon spectrum is *not* primarily related to changes in the magnetic correlations with dop-

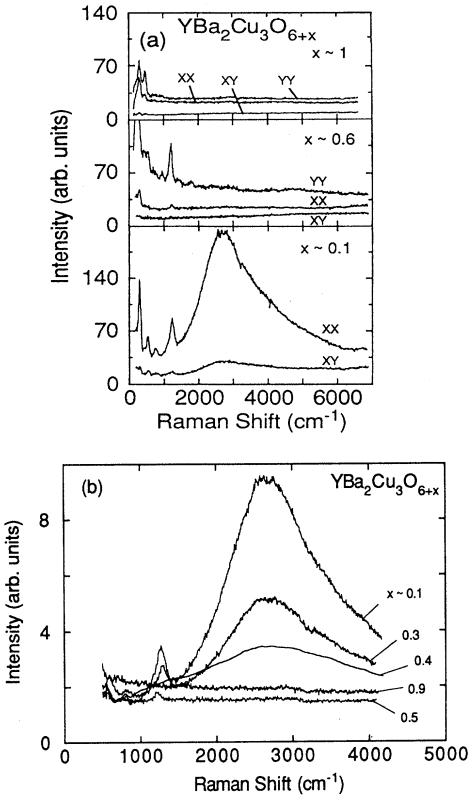


FIG. 9. (a) Raman-scattering spectra in single-domain $YBa_2Cu_3O_{6+x}$ for various $x$. The incident photon energy was $\lambda=488$ nm. The different polarizations measured are $xx$, $yy$, and $xy$, where, for example, $xy$ indicates that the incident photons are polarized along $x$ (parallel to the $a$ axis) and scattered photons are polarized along $y$ (parallel to the $b$ axis). (b) Two-magnon Raman-scattering spectrum as a function of $x$ in $YBa_2Cu_3O_{6+x}$. The spectra have not been corrected for the penetration depth of light in the different samples and the $x\sim0.4$ spectrum has been smoothed.

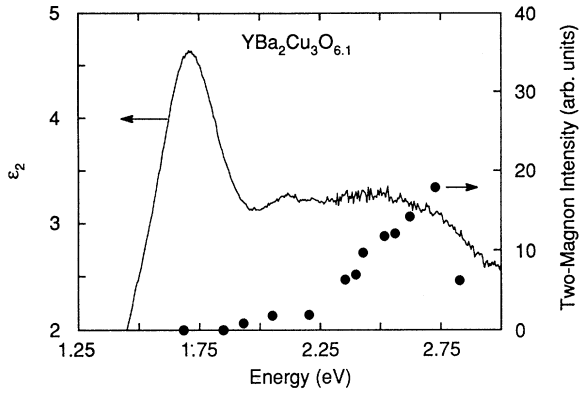


FIG. 10. Comparison of the imaginary part of the dielectric response in $YBa_2Cu_3O_{6.1}$ in the vicinity of the charge-transfer band (solid line) with the integrated intensity of the two-magnon spectrum at various incident frequencies (filled circles).

ing (i.e., via the relationship between two-magnon Raman scattering and the spin-spin-correlation function), but is instead a consequence of the loss of charge-transfer states with decreased doping (see Fig. 5). Models of two-dimensional antiferromagnets in the presence of holes indicate that the dominant effect of hole doping on the spin dynamics is a substantial softening and damping of the spin excitations.[33] However, the two-magnon Raman spectra in $YBa_2Cu_3O_{6+x}$ exhibit little evidence for softening or increased damping as a function of doping below $x\sim0.5$. Therefore, we conclude that the large decrease in two-magnon intensity in this doping range is not primarily related to changes in the spin dynamics. Moreover, Fig. 10 demonstrates that two-magnon scattering in insulating $YBa_2Cu_3O_{6.1}$ is enhanced for incident photon energies in resonance with states in the charge-transfer gap. The diminution of charge-transfer absorption band states with doping is expected to smear this resonance and contribute to a loss of two-magnon intensity. Indeed, a comparison of the Raman spectra and the optical conductivity in Figs. 9(b) and 5(a) demonstrates that there is a strong correlation between the loss of two-magnon Raman intensity and the disappearance of spectral weight in the charge-transfer absorption band with doping in $YBa_2Cu_3O_{6+x}$.

Notably, because the change in two-magnon spectrum with doping in the cuprates appears to be dominated by changes associated with the intermediate states of the two-magnon Raman-scattering process (i.e., the Raman-scattering vertex), the two-magnon Raman spectrum cannot be reliably used to study the effects of doping on the magnetic correlations in these materials. In particular, the disappearance of two-magnon Raman intensity with doping in the cuprates does not refute NMR[34] and neutron-scattering[35] evidence that magnetic correlations persist well into the metallic phase.

## IV. *ab*-PLANE OPTICAL RESPONSE: DISCUSSION

### A. Metal-insulator transition

#### 1. *Redistribution of spectral weight*

One of the most interesting consequences of doping in $YBa_2Cu_3O_{6+x}$ is the transfer of spectral weight from the charge-transfer absorption band to low energies illustrated in Figs. 5(a) and 5(b). This behavior distinguishes the doping dependence in $YBa_2Cu_3O_{6+x}$ from that expected in simple semiconductors, where low-frequency weight grows with the dopant concentration $x$, while spectral weight associated with the fundamental absorption band remains roughly unchanged. A transfer of oscillator strength between different electronic levels with doping is in fact a rather generic feature of the cuprates, having also been observed in optical reflectivity measurements of hole-doped $La_{2-x}Sr_xCuO_4$ (Ref. 1) electron-doped $Nd_{2-x}Ce_xCuO_4$ (Ref. 1) and $Pr_{2-x}Ce_xCuO_4$ (Ref. 2) as well as in x-ray-absorption measurements of $La_{2-x}Sr_xCuO_4$,[36] and resonant photoemission measurements of $Nd_{2-x}Ce_xCuO_4$.[37]

Recent calculations of the optical spectra in both Mott-Hubbard (MH) and $t$-$J$ models demonstrate that a

transfer of spectral weight with doping is a consequence of strong correlations.[38,39] The fundamental absorption band in the insulating phase of the MH model involves the creation of one doubly occupied site and one empty site. Calculations indicate that doping by an amount $x$ causes spectral weight associated with the fundamental absorption to decrease to $1-x$, by creating empty sites and decreasing the probability for creating doubly occupied sites. However, the low-frequency spectral weight induced with doping is *twice* the dopant concentration ($2x$) in the MH picture, since two available states arise from the creation of each empty site.

Electron-doped charge-transfer materials such as the electron-doped cuprates $Nd_{2-x}Ce_xCuO_4$ and $Pr_{2-x}Ce_xCuO_4$ are expected to exhibit a transfer of spectral weight with doping similar to that in the MH picture described above, since electrons are doped primarily onto the Cu sites (i.e., into the upper Hubbard band).[40] On the other hand, *holes* introduced by doping are known to have chiefly oxygen character in the cuprates, and therefore the addition of holes in the O($2p$) band will have no influence on the upper Hubbard band in the absence of O($2p$) and Cu ($3d$) hybridization. Indeed, the development of spectral weight with hole doping in a *localized* charge-transfer system is expected to resemble that of a simple semiconductor. However, Eskes *et al.*[40] have shown that in the presence of finite O($2p$)-Cu($3d$) hopping, spectral weight transfer in hole-doped charge-transfer systems also resembles that of a MH system. In particular, calculations based on charge-transfer models with finite O($2p$)-Cu($3d$) hopping predict an approximate symmetry between electron and hole doping in agreement with experiment,[2] a loss of spectral weight in the fundamental absorption band (i.e., charge-transfer absorption band) with doping, and a growth of low-frequency spectral weight which is larger than the dopant concentration.[40,41] A notable difference between hole- and electron-doped charge-transfer systems, however, is that the amount of low-frequency spectral weight scales with the hopping matrix, $t_{pd}$, in hole-doped systems, while it is relatively insensitive to hybridization strength in electron-doped materials.[40]

In order to compare the predictions of these models with the spectral weight transfer observed in $YBa_2Cu_3O_{6+x}$, we plot in Fig. 11 the integrated spectral weight $N_{\rm eff}$ below $\omega=1.25$ eV, $N_{\rm eff}$ ($\omega=1.25$ eV), as a function of doping for twinned and single-domain $YBa_2Cu_3O_{6+x}$. The effective plasma frequency $\omega_p^2$ [$=8N_{\rm eff}$] associated with this low-frequency spectral weight is shown on the right-hand scale. $N_{\rm eff}$ (1.25 eV) obtained from twinned samples (circles) exhibits a consistent increase with doping, with a dependence given roughly by $N_{\rm eff}\sim 0.9x$. By comparison, $N_{\rm eff}$ (1.25 eV) obtained from the $b$-axis (CuO chain + $CuO_2$ plane) conductivity (triangles) is roughly 25% higher than that obtained on twinned samples, $N_{\rm eff}\sim 1.15$ eV, reflecting the fact that the twinned $YBa_2Cu_3O_{6+x}$ conductivity underestimates the CuO chain conductivity by roughly 50% compared to $b$-axis single-domain results.

The low-frequency spectral weight associated with the $CuO_2$ planes in $YBa_2Cu_3O_{6+x}$ (squares in Fig. 11) exhibits a doping dependence given roughly by $N_{\rm eff}$ (1.25 eV) $\sim 0.65x$. Notably, following our observation that only 50% of the dopant spectral weight goes onto the planes (see Sec. III B 3),[28] we find that the spectral weight growth in the $CuO_2$ planes of $YBa_2Cu_3O_{6+x}$ is approximately 30% larger than the dopant concentration [$N_{\rm eff}$ (1.25 eV) $\sim 1.3x$], in qualitative agreement with the expectations of charge-transfer models.[40] However, the low-frequency spectral weight in the $a$-axis conductivity of $YBa_2Cu_3O_{6+x}$ constitutes a much smaller percentage of the dopant concentration than that observed in $La_{2-x}Sr_xCuO_4$, where the low-frequency spectral weight $N_{\rm eff}$ (1.25 eV) grows with doping according to $N_{\rm eff}$ (1.25 eV) $\sim 2x$ (Ref. 1). There are two principal interpretations of this difference. First, the amount of low-frequency spectral weight in hole-doped charge-transfer systems increases with the degree of O($p$)-Cu($d$) hybridization,[40] suggesting that small differences in O($2p$)-Cu($3d$) hybridization between $YBa_2Cu_3O_{6+x}$ and $La_{2-x}Sr_xCuO_4$ may account for the differences in low-frequency spectral weight growth. However, numerical calculations of $3d$-$2p$ overlaps indicate that the hopping matrix $t_{pd}$ should scale with the in-plane CuO distance, $r$, according to $t_{pd}\sim 1/r^n$, $2.5<n<4$.[42,43] Consequently, the hopping parameter in $YBa_2Cu_3O_{6+x}$ should be only 5–10% smaller than that in $La_{2-x}Sr_xCuO_4$, which is probably insufficient to fully account for the different low-frequency spectral weights observed in these materials.

Alternatively, the greater low-frequency spectral weight in $La_{2-x}Sr_xCuO_4$ with light doping may reflect larger impurity band contributions in this material (and in the 2:1:4 compounds in general), since the presence of an impurity band is also expected to pull spectral weight from the conduction and/or valence bands to lower frequencies. Indeed, as discussed in Sec. IV A 2, the presence of a large mid-IR absorption band and the doping independence of the plasma frequencies observed at intermediate concentrations in the 2:1:4 cuprates provides strong evidence that impurity band contributions

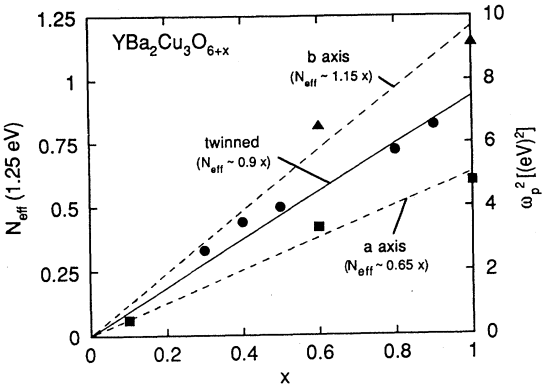


FIG. 11. Scaling of the integrated spectral weight below 1.25 eV, $N_{\rm eff}$ (1.25) [see Eq. (3)] with $x$ in twinned $YBa_2Cu_3O_{6+x}$ (circles), $b$-axis $YBa_2Cu_3O_{6+x}$ [=CuO plane + chain] (triangles), and $a$-axis $YBa_2Cu_3O_{6+x}$ [=$CuO_2$ plane] (squares). The right-hand scale indicates the square of the equivalent plasma frequency ($\sim 8N_{\rm eff}$).

comprise a substantial fraction of the low-frequency spectral weight in these materials.

### 2. *Comparison with other oxide superconductors*

A comparison of the $CuO_2$ plane optical response in $YBa_2Cu_3O_{6+x}$ with that observed in the 2:1:4 cuprates reveals several significant differences. First, the conductivity in the $CuO_2$ planes of the 2:1:4 cuprates exhibits two distinct components, a Drude-like contribution and a large mid-infrared absorption band that shifts to lower energy with increased doping.[1,2] By contrast, no resolvable mid-infrared absorption band is observed in the conductivity of *a*-axis $YBa_2Cu_3O_{6.6}$, *a*-axis $YBa_2Cu_3O_7$ or $Bi_2Sr_2CaCu_2O_8$ below 1 eV (see Fig. 6). Secondly, the squared screened plasma frequency $\omega_p^2$, associated with the $CuO_2$ planes of $YBa_2Cu_3O_{6+x}$, scales linearly with doping (see Fig. 11), while in 2:1:4 compounds such as $La_{2-x}Sr_xCuO_4$, the plasma frequency is relatively insensitive to doping throughout much of the metallic regime.[1] This difference is also apparent when comparing the dielectric response of $YBa_2Cu_3O_{6+x}$ in Fig. 8(a) to that of $La_{2-x}Sr_xCuO_4$, obtained by Uchida *et al.*[1] In $YBa_2Cu_3O_{6+x}$, the zero crossing in the dielectric response increases substantially with doping [see Fig. 8(a)], as expected of a material dominated by free-carrier contributions. However, in $La_{2-x}Sr_xCuO_4$, the zero crossing is pinned near 0.7 eV throughout a wide doping range in the metallic phase, $0.1 \leq x \leq 0.34$, suggesting that positive contributions to $\varepsilon_1$ from *bound* states in the mid-infrared absorption band compete with the negative free-carrier contributions to pin the plasma frequency. Notably, a mid-infrared absorption band of bound carriers dominates the low-frequency spectral weight even more dramatically in $Ba_{1-x}K_xBiO_3$,[44] causing the screened plasma frequency to decrease with increased doping as the mid-infrared absorption band shifts to lower energies.

The differences noted above suggest that bound-carrier contributions comprise a much larger fraction of the spectral weight below 1 eV in the 2:1:4 compounds than in higher $T_c$ materials such as $YBa_2Cu_3O_7$ or $Bi_2Sr_2CaCu_2O_8$. Differences in bound-carrier contributions among the cuprates are also apparent upon examining the relationship between the transition temperature $T_c$ and the integrated spectral weight below 1 eV [$N_{\text{eff}}$ (1 eV)] in different materials. Figure 12 plots $T_c$ vs the $CuO_2$ plane contribution to the spectral weight per unit cell [$\omega_p^2 = N_{\text{eff}}$ (1 eV)] in $Bi_2Sr_2CaCu_2O_8$, *a*-axis $YBa_2Cu_3O_7$, *a*-axis $YBa_2Cu_3O_{6.6}$, and $La_{2-x}Sr_xCuO_4$ (from Ref. 1). Notably, this comparison assumes that the nearest-neighbor $CuO_2$ plane bilayers are the essential structural unit for the superconducting properties in $Bi_2Sr_2CaCu_2O_8$ and $YBa_2Cu_3O_{6+x}$. Figure 12 clearly shows that the value of $\omega_p^2$ in $La_{2-x}Sr_xCuO_4$ falls below the trend in $T_c$ vs $\omega_p^2$ (solid line in Fig. 12) exhibited by *a*-axis $YBa_2Cu_3O_{6.6}$ and *a*-axis $YBa_2Cu_3O_7$. By contrast, all of the cuprates, including the 2:1:4 compounds, have been shown to exhibit a strong correlation between $T_c$ and the superconducting carrier density, $n_s/m^*$.[45] The fact that low-frequency spectral weight in $La_{2-x}Sr_xCu_2O_4$ does not scale in the same way with $T_c$ as that of $YBa_2Cu_3O_{6+x}$ and $Bi_2Sr_2CaCu_2O_8$ (see Fig. 12) supports the conclusion that a larger fraction of the former's spectral weight below 1 eV is comprised of bound carriers not contributing to superconductivity.

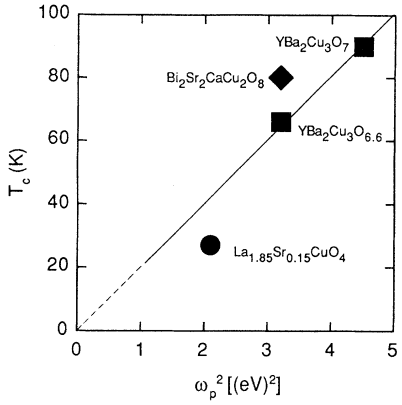


FIG. 12. $T_c$ vs the $CuO_2$ plane contributions to $\omega_p^2$ per unit cell in various cuprate materials, illustrating the scaling of low-frequency spectral weight with $T_c$ $\omega_p^2$ in this plot is derived from the number of effective carriers below 1.25 eV, $N_{\text{eff}}$ (1.25), in Fig. 11.

There are two chief interpretations of the large mid-infrared absorption band observed below the optimal doping concentration ($x \sim 0.15$) in the 2:1:4 cuprates: (1) an incoherent free-carrier contribution, arising from internal degrees of freedom associated with strongly interacting quasiparticles; and (2) a shallow band of impurities. The absence of a strong mid-infrared absorption band in *a*-axis $YBa_2Cu_3O_{6+x}$ or $Bi_2Sr_2CaCu_2O_8$ argues against an incoherent free-carrier contribution in the 2:1:4 compounds, as such a process should be a universal feature of the $CuO_2$ planes in the cuprates. Moreover, the large amount of spectral weight in the mid-infrared absorption band of the 2:1:4 compounds corresponds to an unphysically large interaction strength if interpreted as an incoherent contribution in a Holstein process.[30]

That the mid-infrared absorption band observed in $La_{2-x}Sr_xCuO_4$ at intermediate concentration may be an impurity band is suggested by several features. The predominance of impurity contributions in the 2:1:4 compounds compared to $YBa_2Cu_3O_{6+x}$ is anticipated due to the larger influence that cation/anion disorder should have on the $CuO_2$ planes in the 2:1:4 compounds. Specifically, the dopant sites in $La_{2-x}Sr_xCuO_4$ (i.e., the La/Sr-O planes) are roughly 50% closer to the $CuO_2$ planes than those in the CuO chains of $YBa_2Cu_3O_{6+x}$.[46] Consequently, the disorder potential associated with Sr impurities in $La_{2-x}Sr_xCuO_4$ is expected to have a much more dramatic influence on transport in the $CuO_2$ planes than that associated with vacancies in the CuO chains of $YBa_2Cu_3O_{6+x}$. The presence of a large band of shallow impurities may account in part for the steep slope in the metal-insulator phase boundary of $La_{2-x}Sr_xCuO_4$ (Ref. 47) and $Nd_{2-x}Ce_xCuO_4$ (Ref. 48) since a large impurity

band would cause the mobile density of carriers $n_s$ to be extremely sensitive to changes in the mobility edge as a function of doping.

### B. Charge dynamics in the metallic phase

#### 1. One- vs two-component pictures

Attempts to understand the non-Drude optical conductivity and the broad inelastic Raman-scattering continuum in the metallic phase of $YBa_2Cu_3O_{6+x}$ and other cuprates have given rise to a dichotomy among interpretations of the charge dynamics in these materials. Single-component pictures view the anomalous optical response as a manifestation of quasiparticle interactions, in which the carriers derive a frequency- and temperature-dependent self-energy, the imaginary part of which goes as $\mathrm{Im}\Sigma \sim \max(\omega, T)$. This quasiparticle damping has been proposed to arise either from band-structure features, as in the nested Fermi liquid[49] and Van Hove singularity[50,51] models, or from non-Fermi liquid behavior, as in the marginal Fermi liquid[52] and Luttinger liquid[53] models. Alternatively, two-component models view the non-Drude conductivity as comprised of both a Drude contribution centered at $\omega=0$ and a secondary mid-infrared absorption band arising from bound charges such as interband transitions.

It was suggested in the previous section that a two-component picture is the best description of the $CuO_2$ plane optical response in the 2:1:4 cuprates, based upon the large mid-infrared absorption contribution to the conductivity and the pinning of the plasma frequency $\omega_p$ over a wide doping range. However, in $YBa_2Cu_3O_{6+x}$ and $Bi_2Sr_2CaCu_2O_8$, the absence of a resolvable secondary absorption band in the $CuO_2$ plane conductivity (see Fig. 6) and the systematic scaling of $\omega_p^2$ with doping and $T_c$ (see Fig. 11) provides evidence that the spectral weight below 1 eV in the $CuO_2$ planes of these materials is comprised primarily of a single component of mobile carriers throughout the metallic phase. Additionally, recent microwave,[54] infrared transmission,[55,56] and conductivity[57] results show that the carrier scattering rates in $YBa_2Cu_3O_{6+x}$ and $Bi_2Sr_2CaCu_2O_8$ have anomalous temperature dependences, suggesting that frequency-dependent scattering effects may be large in these materials.

Motivated by these arguments, we analyze the non-Drude optical conductivities of *a*-axis $YBa_2Cu_3O_{6+x}$ ($x \geq 0.6$) and $Bi_2Sr_2CaCu_2O_8$ using a generalized Drude model,

$$\epsilon(\omega)=\epsilon_b-\frac{\omega_p^2}{\omega[m^*(\omega)/m_0][\omega+i/\tau^*(\omega)]} \quad (5)$$

where $\epsilon_b$ represents bound contributions to the dielectric response (assumed small), and the second term represents the effects of frequency-dependent damping of the carriers, with $m^*(\omega)/m_0$ representing the effective-mass enhancement over the band mass and $1/\tau^*(\omega) = 1/\tau(\omega)[m/m^*(\omega)]$ representing the renormalized quasiparticle scattering rate. Figure 13 illustrates the resulting frequency-dependent scattering rates of *a*-axis $YBa_2Cu_3O_{6.6}$ (filled triangles), *a*-axis $YBa_2Cu_3O_7$ (open triangles), and $Bi_2Sr_2CaCu_2O_8$ (circles) below 0.3 eV. The effective-mass enhancements in *a*-axis $YBa_2Cu_3O_{6+x}$ are also shown in the inset.

The single-component analysis in Fig. 13 has two interesting results. First, the frequency-dependent scattering rates of *a*-axis $YBa_2Cu_3O_{6+x}$ and $Bi_2Sr_2CaCu_2O_8$ have a linear-in-$\omega$ dependence below 0.5 eV. This well-known result is consistent with numerous models of the normal state in which strong quasiparticle damping is assumed.[49–53] More significantly, the slope of the linear-in-$\omega$ scattering rate roughly scales with decreased carrier density in the single-component picture, implying that there is an increase in the quasiparticle interaction strength $\lambda$ with decreased doping. This result is consistent with models in which the quasiparticle mass is enhanced by strong correlation effects (for example, via the Coulomb interaction[58]) as the dopant concentration is reduced towards the insulating phase. Further, that the maximum value of $T_c$ in $YBa_2Cu_3O_{6+x}$ does not correspond to the maximum value of the quasiparticle interaction strength $\lambda$ appears to suggest that too much quasiparticle scattering is detrimental to superconductivity in the cuprates.[59]

#### 2. Relationship to Raman scattering

Additional insight into the nature of the normal state in the cuprates is afforded by an examination of the unusual Raman-scattering continuum[4–6] [see Fig. 9(a)], and its relationship with the non-Drude optical conductivity. Raman scattering from free carriers in a conventional metal or doped semiconductor is strongly constrained by the *f*-sum rule.[60] The Raman-scattering response function $\mathrm{Im}R(q=0,\omega)$, in this case, exhibits a high-energy cutoff near $qv_F$ and a strongly suppressed intensity due to screening. By contrast, the Raman continuum [see Fig. 9(a)] in the cuprates appears not to be con-

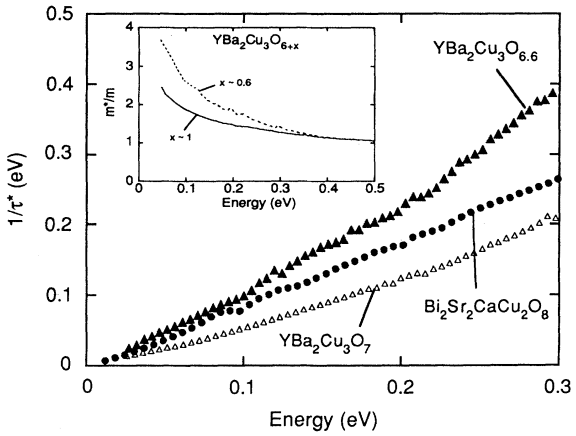


FIG. 13. Renormalized scattering rate $1/\tau^*$ for *a*-axis $YBa_2Cu_3O_7$ (open triangles), *a*-axis $YBa_2Cu_3O_{6.6}$ (filled triangles), and $Bi_2Sr_2CaCu_2O_8$, derived from the complex conductivity using Eq. (5). Inset, effective-mass enhancements $m^*/m$ for *a*-axis $YBa_2Cu_3O_{6+x}$.

strained by a known sum rule, exhibiting an extremely strong scattering intensity and an energy range that extends at least an order of magnitude farther than $qv_F$ ($\sim 100\,\mathrm{cm}^{-1}$).

The chief explanations for the unusual behavior in the cuprates have been that either (1) the continuum arises from spin excitations or from some unusual polarizability,[52] or (2) one of a number of conditions under which the $f$-sum rule for electronic Raman scattering can be avoided[61] is present in the cuprates, such as impurities,[62] strong inelastic scattering, interband transitions,[63] frequency-dependent damping from electron-electron interactions,[64,49] or Fermi surface anisotropy.[65] Many of these alternatives make specific predictions about either the frequency dependence of the Raman-scattering response, or the relationship between the Raman-scattering continuum and the optical conductivity, that can be tested by our results. For example, Raman scattering in the presence of disorder cannot account for the broad, flat continuum in the cuprates, since the scattering response in the presence of impurities is expected to peak at an energy on the order of the scattering rate.[62] Moreover, electronic Raman scattering from interband transitions should be sensitive to details of the band structure, and thus could not easily explain the diversity of cuprates in which a continuum is observed.[5]

One of the most interesting properties of the room-temperature Raman continuum in $YBa_2Cu_3O_{6+x}$ is its insensitivity to doping [see Fig. 9(a)]. By contrast, the $a$-axis optical conductivity increases significantly with increased doping (see Fig. 6). The doping independence of the *ab*-plane Raman continuum suggests two alternative interpretations of the relationship between the Raman continuum and the optical response. One possibility is that most of the Raman continuum intensity is not associated with the conduction electrons, and thus is not related to the non-Drude optical conductivity.[12] A second possibility is that the Raman continuum is associated with the conduction electrons, and its doping independence reflects changes in the Raman-scattering vertex. In particular, under general circumstances electronic Raman scattering couples to fluctuations in an *effective* charge density,[61] which should scale with the degree of local Fermi surface anisotropy. Consequently, the absence of a doping dependence in the Raman continuum in the metallic phase could result either from increased Fermi surface anisotropy, or decreased *screening* of anisotropy, with decreased doping. Unfortunately, until a better understanding of the Raman-scattering vertex associated with the *ab*-plane continuum is obtained, this issue will be difficult to resolve.

## V. *c*-AXIS OPTICAL RESPONSE: RESULTS AND DISCUSSION

The nature of the charge dynamics along the $c$ axis is also of great importance, as it underlies the basic assumptions of many normal and superconducting state models of the layered cuprates. An important issue remains whether charge transport along the $c$ direction is coherent. In order to address this issue, we have examined thick $c$-axis samples of $YBa_2Cu_3O_{6+x}$ as a function of $x$ using optical reflectivity and Raman scattering.[60]

The low-frequency ($0.01 < \omega < 0.5$ eV) optical reflectivity for light polarized along the $c$ direction of single-crystal $YBa_2Cu_3O_{6+x}$ is illustrated in Fig. 14(a) for several values of $x$. The high-frequency optical response ($0.01 < \omega < 5$ eV) is compared in the inset. The $c$-axis reflectivity of $YBa_2Cu_3O_7$ ($T_c = 91$ K) exhibits a weak Drude-like metallic response, as well as $c$-axis phonons at 156, 195, 283, 320, and 572 $\mathrm{cm}^{-1}$, in agreement with the results of previous $c$-axis studies.[67,68] The corresponding $c$-axis conductivity in $YBa_2Cu_3O_7$ is illustrated in Fig. 14(b) (top curves), obtained from a Kramers-Kronig analysis of the reflectivity data. The optical response of $YBa_2Cu_3O_7$ below 0.5 eV in Fig. 14 can be nicely described by a three-component model comprised of a Drude contribution with plasma frequency, scattering rate, and high-frequency dielectric response given by $\omega_{pD} = 4150\ \mathrm{cm}^{-1}$ (0.51 eV), $\Gamma_D = 1800\ \mathrm{cm}^{-1}$ (0.22 eV), and $\epsilon_\infty = 5$, and two mid-infrared oscillators having frequencies, damping rates, and effective plasma frequencies given by $\omega_{01} = 2400\ \mathrm{cm}^{-1}$, $\Gamma_1 = 3300\ \mathrm{cm}^{-1}$, $\omega_{p1} = 4800$

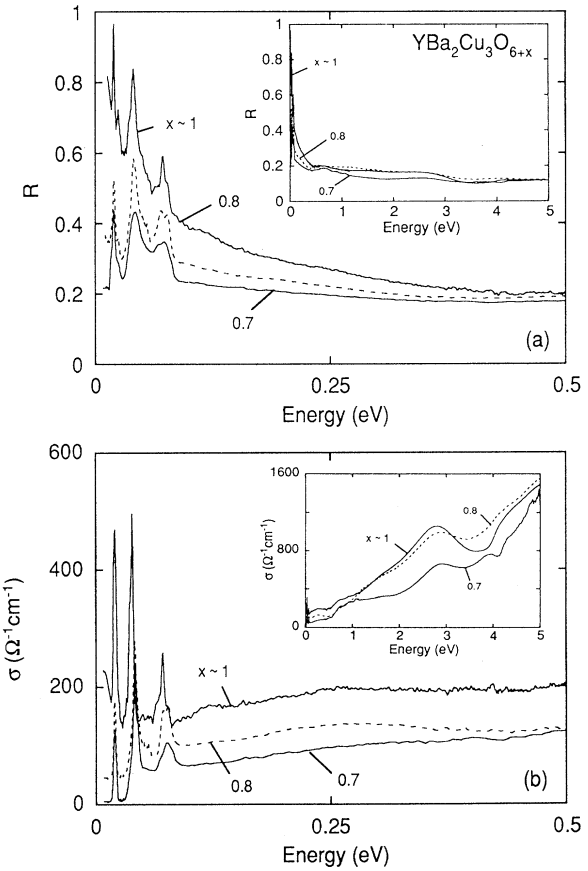


FIG. 14. (a) Low-frequency ($0.012 \le \omega \le 0.5$ eV) $c$-axis reflectivity of $YBa_2Cu_3O_{6+x}$ for several $x$ at room temperature. The inset illustrates the reflectivity up to 5 eV. (b) Real part of the optical conductivity $\sigma$ ($0.012 \le \omega \le 0.5$ eV) of $c$-axis $YBa_2Cu_3O_{6+x}$ for several $x$. The inset illustrates $\sigma$ up to 5 eV.

$cm^{-1}$, $\omega_{02}=6000$ $cm^{-1}$, $\Gamma_2=4000$ $cm^{-1}$, $\omega_{p2}=4400$ $cm^{-1}$. The Drude parameters in $YBa_2Cu_3O_7$ correspond to a dc conductivity of $\sigma(0)\sim 160\ \Omega^{-1}cm^{-1}$, which is quite consistent with the zero-frequency extrapolation of the $c$-axis conductivity from the Kramers-Kronig analysis in Fig. 14(b), $\sigma(0)\sim 200\ \Omega^{-1}cm^{-1}$. Notably, these dc conductivities are much less than the limit proposed by Mott[69] for coherent conduction, suggesting that $c$-axis transport in $YBa_2Cu_3O_7$ may result from incoherent hopping. Indeed, an estimate of the mean free path for $c$-axis transport, $l=4\pi\sigma(0)v_F/\omega_p^2$, gives a value that is substantially less than the $c$-axis lattice parameter.[68]

It is interesting to compare the $c$-axis optical conductivity to the $c$-axis Raman-scattering response in $YBa_2Cu_3O_7$ ($T_c\sim 90$ K) [$\mathbf{E}_i,\mathbf{E}_s\|c$ axis]. Figure 15 illustrates that the $c$-axis Raman response is characterized by a broad $c$-axis polarized continuum, which we attribute to electronic scattering from the carriers responsible for the Drude conductivity (see Fig. 14, top curve). The $c$-axis Raman continuum can be approximately described by the response function (smooth solid line)

$$\mathrm{Im}R(\omega)\sim\frac{\omega\Gamma}{\omega^2+\Gamma^2}\ , \tag{6}$$

suggesting that carrier scattering along the $c$ direction is simple relaxational with a characteristic damping rate on the order of $\Gamma\sim 1000$ $cm^{-1}$. This response function is consistent with a carrier scattering process having a characteristic $c$-axis scattering rate, $\Gamma$. Several unconventional properties of the $c$-axis optical response suggest that $c$-axis scattering cannot arise from impurities. First, the short mean free path estimated from the optical data ($l<a$)[68] argues that the Raman continuum does not result from a conventional phonon- or impurity-assisted process. Further, the optical response does not show a peak at the impurity scattering rate as expected of a dirty metal, also suggesting that the $c$-axis continuum does not arise from simple impurity scattering. Finally, it is difficult to reconcile the presence of strong $c$-axis impurity scattering with $a$-axis conductivities which are in the clean limit.[3]

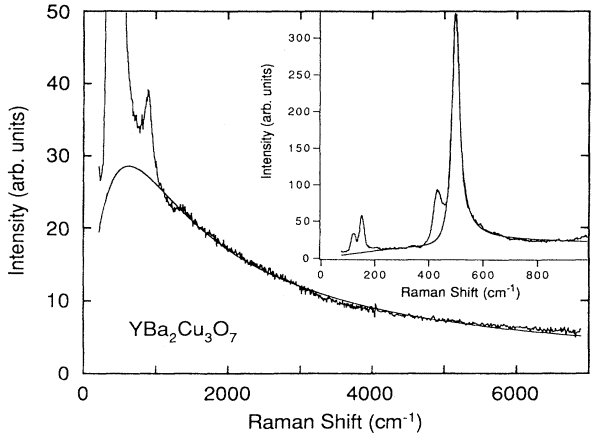


FIG. 15. Room-temperature Raman scattering in $YBa_2Cu_3O_7$ with incident and scattered light polarizations along the $c$ axis [$=(zz)$]. The smooth solid line is a fit to the data using the simple relaxational response in Eq. (6). The inset illustrates the low-frequency phonons for the $(zz)$ scattering geometry.

An alternative interpretation for the $c$-axis optical response is motivated by recent suggestions that $c$-axis charge transport in the highly layered cuprates may be strongly influenced by in-plane energy fluctuations.[70] Specifically, Leggett has pointed out that due to the large anisotropy associated with the cuprates, in-plane thermal fluctuations can break the band degeneracy between adjacent $CuO_2$ layers by energies larger than the $c$-axis hopping rate, thereby destroying coherent transport in the $c$ direction.[70] This process is consistent with the observation of a low conductivity perpendicular to the highly conducting layers of $YBa_2Cu_3O_7$, since uncorrelated fluctuations in the energy in adjacent bilayers should dephase the electronic wave function each time the carrier hops to a different bilayer. An interesting consequence of this "dynamical dephasing" process is that the $c$-axis scattering rate should be strongly influenced by the nature of the *in-plane dynamics.* Indeed, the $c$-axis scattering rate in the $c$-axis Drude response and Raman continuum in the presence of dynamical dephasing should be roughly a measure of the imaginary part of the self-energy *associated with excitations* in the $CuO_2$ planes. Consequently, $c$-axis measurements may be extremely useful in probing the nature and origin of the unusual charge dynamics in the $CuO_2$ planes.

Upon decreasing the doping level slightly within the metallic phase, the $c$-axis optical reflectivity in Fig. 14(a) develops increasingly insulating behavior. This doping dependence is also illustrated [see Fig. 14(b)] by the rapid decrease in the $c$-axis optical conductivity with decreasing doping. In particular, the extrapolation of the zero-frequency conductivity in $c$-axis $YBa_2Cu_3O_{6+x}$ decreases from $\sigma(0)\sim 200\ \Omega^{-1}cm^{-1}$ in $YBa_2Cu_3O_7$ ($T_c=91$ K) to less than $50\ \Omega^{-1}cm^{-1}$ in $YBa_2Cu_3O_{6.8}$ ($T_c=81$ K), and to roughly $0\ \Omega^{-1}cm^{-1}$ in $YBa_2Cu_3O_{6.7}$ ($T_c=70$ K). This trend reflects a decrease in the $c$-axis hopping conductivity, and is consistent with an increase in two dimensionality with decreased doping in $YBa_2Cu_3O_{6+x}$. A trend towards increased two dimensionality with decreased doping has also been inferred from transport,[71] magnetic,[72] and heat-capacity[73] measurements.

Notably, the fact that the *ab*-plane response in Figs. 11 and 12 changes only slightly over the doping range $x\sim 1$ to $x\sim 0.6$ argues that $c$-axis coupling *within* each $CuO_2$ plane bilayer is essentially preserved with decreased doping (albeit with a smaller carrier density). Therefore, the decrease in $c$-axis coupling with decreased doping in $YBa_2Cu_3O_{6+x}$ appears to arise from a decoupling of *adjacent* $CuO_2$ bilayers, apparently due to a degradation of the CuO chains. More significantly, the charge dynamics characterizing the *ab* planes appear to be relatively insensitive to the decoupling of the $CuO_2$ bilayers with decreased doping (see Fig. 6). Indeed, the single-component analysis in Fig. 13 indicates that frequency-dependent scattering rate associated with the $CuO_2$ planes remains linear ($1/\tau\sim\omega$) over the doping range $x\sim 1$ to $x\sim 0.6$. This result provides strong evidence that the nature of

the unusual *ab*-plane charge dynamics is insensitive to interbilayer coupling. Thus, the spin or charge excitations responsible for the anomalous $CuO_2$ plane charge dynamics in $YBa_2Cu_3O_{6+x}$ appear to persist in nearly isolated $CuO_2$ bilayers. Significantly, transport measurements of $YBa_2Cu_3O_{6+x}/PrBa_2Cu_3O_{6+x}$ superlattices have shown that *superconductivity* persists in nearly decoupled pairs of $CuO_2$ bilayers,[74] corroborating the strongly two-dimensional nature of the electronic states in $YBa_2Cu_3O_{6+x}$.

## VI. SUMMARY

In this paper, we have examined the detailed relationship between the Raman scattering and optical responses in $YBa_2Cu_3O_{6+x}$ in order to elucidate the nature of the optical response in various phase regimes. Upon doping across the metal-insulator transition, we find that spectral weight in the $CuO_2$ planes of $YBa_2Cu_3O_{6+x}$ develops in a manner consistent with Hubbard model predictions. For example, spectral weight in the fundamental (charge-transfer) absorption band of $YBa_2Cu_3O_{6+x}$ is transferred to low frequencies with doping, and the development of low-frequency spectral weight in the $CuO_2$ planes of $YBa_2Cu_3O_{6+x}$ is slightly larger than that anticipated from the dopant concentration [$N_{\rm eff}$ (1.25 eV) $> x$]. However, we find that these effects are less dramatic than in $La_{2-x}Sr_xCuO_4$, possibly due to the effects of smaller O(2*p*)-Cu(3*d*) hybridization or smaller impurity band contributions in $YBa_2Cu_3O_{6+x}$. We also find that the decrease of two-magnon Raman-scattering intensity with doping is primarily related to the loss of charge-transfer states, and *not* to changes in magnetic correlations with doping. Thus Raman-scattering measurements are not in conflict with neutron scattering or NMR with respect to the presence of magnetic correlations in the metallic phase.

We also show that the optical response in the $CuO_2$ planes of different cuprates varies quite dramatically. In particular, our results suggest that bound-carrier contributions comprise a substantially larger fraction of the low-frequency spectral weight in the lower-$T_c$ cuprates (e.g., the 2:1:4 compounds) than in higher-$T_c$ cuprates such as $YBa_2Cu_3O_{6+x}$ and $Bi_2Sr_2CaCu_2O_8$. We attribute the bound mid-infrared contributions in the 2:1:4 compounds to an impurity band, and argue that the presence of this band may play a significant role in determining the phase diagrams and transition temperatures of these materials. Our results also imply that the low-frequency spectral weight in the 2:1:4 compounds is best described by a two-component picture involving mobile and bound-carrier contributions.

In the metallic phase of higher-$T_c$ cuprates such as $YBa_2Cu_3O_{6+x}$ and $Bi_2Sr_2CaCu_2O_8$, there is still no definitive evidence in support of either a single- or two-component picture of the low-frequency spectral weight. However, we argue that a single-component picture is a good description of the low-frequency spectral weight in $YBa_2Cu_3O_{6+x}$ based on both the scaling of the low-frequency spectral weight with both doping and $T_c$, and the absence of a resolvable bound-carrier contribution in the low-frequency conductivity. We also find that a strict interpretation of the optical data within a single-component picture has several interesting consequences, including an increase in the interaction strength $\lambda$ with decreasing $T_c$. Whether normal-state models can accommodate these results remains an open question. Additionally, the doping independence of the Raman-scattering continuum places constraints on its possible relationship to the optical response, suggesting either that the Raman-scattering continuum is not associated with the conduction electrons, or that fundamental changes in the Raman-scattering vertex occur with decreased doping.

Finally, in our *c*-axis studies, we find that the *c*-axis optical response in fully oxygenated $YBa_2Cu_3O_7$ ($T_c \sim 90$ K) is characterized by a weak Drude conductivity and a *c*-axis polarized Raman continuum. Both optical responses are consistent with incoherent hopping transport along the *c* direction, which we argue is due to a dephasing of *c*-axis transport by uncorrelated dynamical fluctuations in adjacent $CuO_2$ plane layers. We suggest that this unconventional dephasing process should allow one to probe the dynamics in the *ab* plane using *c*-axis measurements. With decreased doping in the metallic phase, we find that the $CuO_2$ bilayers become rapidly decoupled due to the loss of oxygens in the CuO chains. The unusual *ab*-plane optical response appears to be rather insensitive to interbilayer decoupling, providing evidence that the normal-state dynamics which characterize the $CuO_2$ planes persist in nearly isolated $CuO_2$ bilayers.

## ACKNOWLEDGMENTS

The authors would like to acknowledge very useful conversations with E. Dagotto, D. Frenkel, M. S. Hybertsen, A. J. Leggett, R. Martin, A. J. Millis, T. M. Rice, T. Timusk, and D. Wake. We would also like to thank S.-W. Cheong of AT&T Bell Labs for the $Gd_2CuO_4$ samples, and P. Nyhus, A. V. Bazherov, A. A. Maksimov, A. V. Puchkov, and I. I. Tartakovskii for technical assistance on some of the Raman-scattering measurements. This work was supported by the National Science Foundation (Grant No. 90-20000) through the Science and Technology Center for Superconductivity and in part by the U.S. Department of Energy, Basic Energy Sciences-Materials Science Division (Contract No. W-31-109-Eng-38). One of us (M.A.K.) acknowledges support from the Department of Defense.

[1]S. Uchida, T. Ido, H. Takagi, T. Arima, Y. Tokura, S. Tajima, Phys. Rev. B **43**, 7942 (1991).

[2]S. L. Cooper, G. A. Thomas, D. H. Rapkine, A. J. Millis, S.-W. Cheong, A. S. Cooper, and Z. Fisk, Phys. Rev. B **42**, 6342 (1990).

[3]For a review, see D. B. Tanner and T. Timusk, in *Physical Properties of High Temperature Superconductors III*, edited by D. M. Ginsberg (World Scientific, Singapore, 1992), and references therein.

[4]S. L. Cooper and M. V. Klein, Comments Condens. Matter Phys. **15**, 99 (1990), and references therein.

[5]S. Sugai, in *Mechanisms of High Temperature Superconductivi-*

*ty*, edited by H. Kamimura and A. Oshiyama (Springer-Verlag, Heidelberg, 1989).
[6]C. Thomsen and M. Cardona, in *Physical Properties of High Temperature Superconductors*, edited by D. M. Ginsberg (World Scientific, Singapore, 1989), p. 409, and references therein.
[7]J. P. Rice and D. M. Ginsberg, J. Cryst. Growth **109**, 432 (1991).
[8]W. C. Lee and D. M. Ginsberg, Phys. Rev. B **44**, 2815 (1991).
[9]B. W. Veal, A. P. Paulikas, Hoydoo You, Hao Shi, Y. Fang, and J. W. Downey, Phys. Rev. B **42**, 6305 (1990).
[10]F. Stern, *Solid State Physics* (Academic, New York, 1963), Vol. 15.
[11]I. Bozovic, Phys. Rev. B **42**, 1969 (1990).
[12]D. Reznik, M. V. Klein, W. C. Lee, D. M. Ginsberg, and S.-W. Cheong, Phys. Rev. B **46**, 11 725 (1992).
[13]J. Zaanen, G. A. Sawatzky, and J. W. Allen, Phys. Rev. Lett. **55**, 418 (1985).
[14]N. Nücker, H. Romberg, X. X. Xi, J. Fink, B. Gegenheimer, and Z. X. Zhao, Phys. Rev. B **39**, 6619 (1989); M. Alexander, H. Romberg, N. Nücker, P. Adelmann, J. Fink, J. T. Markert, M. B. Maple, S. Uchida, H. Takagi, Y. Tokura, A. C. W. P. James, and D. W. Murphy, *ibid.* **43**, 333 (1991).
[15]R. M. Hazen, in *Physical Properties of High Temperature Superconductors II*, edited by D. M. Ginsberg (World Scientific, Singapore, 1990), p. 121.
[16]A. Fujimori, E. Takayama-Muromuchi, Y. Uchida, and B. Okai, Phys. Rev. B **35**, 8814 (1987).
[17]S. L. Cooper, G. A. Thomas, J. Orenstein, D. H. Rapkine, A. J. Millis, S.-W. Cheong, and Z. Fisk, Phys. Rev. B **41**, 11 605 (1990).
[18]Y. Tokura, H. Takagi, T. Arima, S. Koshihara, T. Ido, S. Ishibashi, and S. Uchida, Physica C **162-164**, 1231 (1989).
[19]M. S. Hybertsen, M. Schluter, and N. E. Christensen, Phys. Rev. B **39**, 9028 (1989).
[20]E. B. Stechel and D. R. Jennison, Phys. Rev. B **38**, 4632 (1988).
[21]J. Kircher, M. K. Kelly, S. Rashkeev, M. Alouani, D. Fuchs, and M. Cardona, Phys. Rev. B **44**, 217 (1991).
[22]M. K. Kelly, P. Barboux, J.-M. Tarascon, D. E. Aspnes, W. A. Bonner, and P. A. Morris, Phys. Rev. B **38**, 870 (1988).
[23]M. Garriga, J. Humlicek, M. Cardona, and E. Schonherr, Solid State Commun. **66**, 1231 (1988).
[24]T. Arima, K. Kikuchi, M. Kasuya, S. Koshihara, Y. Tokura, T. Ido, and S. Uchida, Phys. Rev. B **44**, 917 (1991).
[25]B. Koch, H. P. Geserich, and Th. Wolf, Solid State Commun. **71**, 495 (1989).
[26]M. P. Petrov, A. I. Grachev, M. V. Krasin'kova, A. A. Nechitailov, V. V. Poborchii, S. I. Shagin, and S. V. Miridonov, Pis'ma Zh. Eksp. Teor. Fiz. **50**, 25 (1989) [JETP Lett. **50**, 29 (1989)].
[27]Z. Schlesinger, R. T. Collins, F. Holtzberg, C. Field, S. H. Blanton, U. Welp, G. W. Crabtree, and Y. Fang, Phys. Rev. Lett. **65**, 801 (1990).
[28]S. L. Cooper, A. L. Kotz, M. A. Karlow, M. V. Klein, W. C. Lee, J. Giapintzakis, and D. M. Ginsberg, Phys. Rev. B **45**, 2549 (1992).
[29]L. D. Rotter, Z. Schlesinger, R. T. Collins, F. Holtzberg, C. Field, U. Welp, G. W. Crabtree, J. Z. Kiu, and Y. Fang, G. Vandervoort, and S. Fleshler, Phys. Rev. Lett. **67**, 2741 (1991).
[30]J. Orenstein, G. A. THomas, A. J. Millis, S. L. Cooper, D. H. Rapkine, T. Timusk, L. Schneemeyer, and J. V. Waszczak, Phys. Rev. B **42**, 6342 (1990).
[31]K. B. Lyons, P. A. Fleury, J. P. Remeika, A. S. Cooper, and T. J. Negran, Phys. Rev. B **37**, 2353 (1987); K. B. Lyons, P. A. Fleury, L. E. Schneemeyer, and J. V. Waszczak, Phys. Rev. Lett. **60**, 732 (1988); P. E. Sulewski, P. A. Fleury, K. B. Lyons, S.-W. Cheong, and Z. Fisk, Phys. Rev. B **41**, 225 (1990).
[32]D. M. Krol, M. Stavola, L. F. Schneemeyer, J. V. Waszczak, H. O'Bryan, and S. A. Sunshine, Phys. Rev. B **38**, 11 346 (1988).
[33]I. R. Pimentel and R. Orbach, Phys. Rev. B **46**, 2920 (1992).
[34]T. Imai, T. Shimizu, H. Yasuoka, Y. Ueda, T. Takabatake, Y. Nakazawa, and M. Ishikawa, J. Phys. Soc. Jpn. **57**, 1771 (1988); T. Imai, H. Yasuoka, T. Shimizu, Y. Ueda, K. Yoshimura, and K. Kosuge, Physica C **162-164**, 169 (1989).
[35]J. Rossat-Mignod *et al.*, Physica B **163**, 4 (1990).
[36]C. T Chen, F. Sette, Y. Ma, M. S. Hybertsen, E. B. Stechel, W. M. C. Foulkes, M. Schluter, S.-W. Cheong, A. S. Cooper, L. W. Rupp, Jr., B. Batlogg, Y. L. Soo, Z. H. Ming, A. Krol, and Y. H. Kao, Phys. Rev. Lett. **66**, 104 (1991).
[37]J. W. Allen, C. G. Olson, M. B. Maple, J.-S. Kang, L. Z. Liu, J.-H. Park, R. O. Anderson, W. P. Ellis, J. T. Markert, Y. Kalichaouch, and R. Liu, Phys. Rev. Lett. **64**, 595 (1990).
[38]E. Dagotto, A. Moreo, R. Joynt, S. Bacci, and E. Gagliano, Phys. Rev. B **41**, 2585 (1990); E. Dagotto, A. Moreo, F. Ortolani, J. Riera, and D. J. Scalapino, *ibid.* **45**, 10 107 (1992).
[39]W. Stephan and P. Horsch, Phys. Rev. B **42**, 8736 (1990).
[40]H. Eskes, M. B. J. Meinders, and G. A. Sawatzky, Phys. Rev. Lett. **67**, 1035 (1991); G. A. Sawatzky (unpublished).
[41]M. S. Hybertsen, E. V. Stechel, W. M. C. Foulkes, and M. Schlüter, Phys. Rev. B **45**, 10 032 (1992); M. S. Hybertsen, E. B. Stechel, M. Schluter, and D. R. Jennison, *ibid.* **41**, 11 068 (1990).
[42]K. N. Shrivastava and V. Jaccarino, Phys. Rev. B **13**, 299 (1976).
[43]L. J. de Jongh and R. Block, Physica **79B**, 568 (1975).
[44]M. A. Karlow, S. L. Cooper, A. L. Kotz, M. V. Klein, P. D. Han, and D. A. Payne (unpublished).
[45]Y. J. Uemura *et al.*, Phys. Rev. Lett. **62**, 2317 (1989).
[46]G. A. Thomas, D. H. Rapkine, S. L. Cooper, S.-W. Cheong, A. S. Cooper, L. F. Schneemeyer, and J. V. Waszczak, Phys. Rev. B **45**, 2474 (1992).
[47]H. Takagi, R. J. Cava, M. Marezio, B. Batlogg, J. J. Krajewski, W. F. Peck, Jr., P. Bordet, and D. E. Cox, Phys. Rev. Lett. **68**, 3777 (1992).
[48]S. Uchida, H. Takagi, Y. Tokura, N. Koshihara, and T. Arima, in *Strong Correlation and Superconductivity*, edited by H. Fukuyama, S. Maekawa, and A. Malozemoff (Springer-Verlag, Berlin, 1989), p. 194.
[49]A. Virosztek and J. Ruvalds, Phys. Rev. B **42**, 4064 (1990); J. Ruvalds and A. Virosztek, *ibid.* **43**, 5498 (1991).
[50]P. A. Lee and N. Read, Phys. Rev. Lett. **58**, 2691 (1987).
[51]C. C. Tsuei, D. M. Newns, C. C. Chi, and P. C. Pattnaik, Phys. Rev. Lett. **65**, 2724 (1990); D. M. Newns, P. C. Pattnaik, and C. C. Tsuei, Phys. Rev. B **43**, 3075 (1991).
[52]C. M. Varma, P. B. Littlewood, S. Schmitt-Rink, E. Abrahams, and A. Ruckenstein, Phys. Rev. Lett. **63**, 1996 (1989); P. B Littlewood and C. M. Varma, J. Appl. Phys. **69**, 4979 (1991).
[53]P. W. Anderson, Science **235**, 1196 (1987); P. W. Anderson, in *Strong Correlation and Superconductivity*, edited by H. Fukuyama, S. Maekawa, and A. Malozemoff (Springer-Verlag, Berlin, 1989), p. 2; P. W. Anderson, Phys. Rev. Lett. **64**, 1839 (1990).
[54]D. A. Bonn, P. Dosanjh, R. Liang, and W. N. Hardy, Phys.

Rev. Lett. **68**, 2390 (1992).
[55]D. B. Romero, C. D. Porter, D. B. Tanner, L. Forro, D. Mandrus, L. Mihaly, G. L. Carr, and G. P. Williams, Phys. Rev. Lett. **68**, 1590 (1992).
[56]F. Gao, G. L. Carr, C. D. Porter, and D. B. Tanner, S. Etemad, T. Venkatesan, A. Inam, B. Dutta, X. D. Wu, G. P. Williams, and C. J. Hirschmugl, Phys. Rev. B **43**, 10 383 (1991).
[57]M. C. Nuss, P. M. Mankiewich, M. L. O'Malley, E. H. Westerwick, and P. B. Littlewood, Phys. Rev. Lett. **66**, 3305 (1991).
[58]W. F. Brinkman and T. M. Rice, Phys. Rev. B **2**, 4302 (1970).
[59]P. B. Allen, Comments Condens. Mater. Phys. **15**, 327 (1992).
[60]J. Kosztin and A. Zawadowski, Solid State Commun. **78**, 1029 (1991).
[61]Under these conditions, Raman scattering measures fluctuations are an *effective* charge density that is a local property of the Fermi surface and hence does not commute with the full Hamiltonian. The Raman-scattering response therefore is not constrained by the $f$-sum rule. See, for example, Ref. 65.
[62]A. Zawadowski and M. Cardona, Phys. Rev. B **42**, 10 732 (1990).
[63]H. Monien and A. Zawadowski, Phys. Rev. Lett. **63**, 911 (1989).
[64]B. S. Shastry and B. I. Shraiman, Phys. Rev. Lett. **65**, 1068 (1990).
[65]A. A. Abrikosov and V. M. Genkin, Zh. Eksp. Teor. Fiz. **65**, 842 (1973) [Sov. Phys. JETP **38**, 417 (1974)].
[66]S. L. Cooper, D. Reznik, P. Nyhus, M. V. Klein, W. C. Lee, D. M. Ginsberg, B. W. Veal, A. P. Paulikas, and B. Dabroski (unpublished).
[67]R. T. Collins, Z. Schlesinger, F. Holtzberg, and C. Field, Phys. Rev. Lett. **63**, 422 (1989).
[68]C. C. Homes, N. Cao, T. Timusk, R. Liang, and W. N. Hardy (unpublished).
[69]N. F. Mott and E. A. Davis, *Electronic Processes in Non-Crystalline Materials* (Clarendon, Oxford, 1971).
[70]A. J. Leggett (unpublished).
[71]D. A. Brawner, Z. Z. Wang, and N. P. Ong, Phys. Rev. B **40**, 9329 (1989).
[72]K. E. Gray, D. H. Kim, B. W. Veal, G. T. Seidler, T. F. Rosenbaum, and D. E. Farrell, Phys. Rev. B **45**, 10 071 (1992).
[73]K. Ghiron, M. B. Salamon, B. W. Veal, A. P. Paulikas, and J. W. Downey, Phys. Rev. B **46**, 5837 (1992).
[74]D. H. Lowndes, D. P. Norton, and J. D. Budai, Phys. Rev. Lett. **65**, 1160 (1990).